Domain Decomposition Scheme in Newmark-Beta-FDTD for Dispersive Grating Calculation

Sheng-Bing Shi, Wei Shao, and Kai Wang

School of Physics
University of Electronic Science and Technology of China, Chengdu, 610054, China
shengbing77@163.com, weishao@uestc.edu.cn, wkaiuestc2016@163.com

Abstract ─ In this work, an efficient domain decomposition scheme is introduced into the unconditionally stable finite-difference time-domain (FDTD) method based on the Newmark-Beta algorithm. The entire computational domain is decomposed into several subdomains, and thus the large sparse matrix equation produced by the implicit FDTD method can be divided into some independent small ones, resulting in a fast speed lower-upper decomposition and backward substitution. The domain decomposition scheme with different subdomain schemes and different subdomain numbers is studied. With a generalized auxiliary differential equation (ADE) technique, the extraordinary optical transmission through a periodic metallic grating with bumps and cuts is investigated with the domain decomposition Newmark-Beta-FDTD. Compared with the traditional ADE-FDTD method and the ADE-Newmark-Beta-FDTD method, the results from the proposed method show its accuracy and efficiency.

Index Terms ─ Domain decomposition, extraordinary optical transmission (EOT), Newmark-Beta-FDTD, surface plasmons.

I. INTRODUCTION

Enhanced transmission through subwavelength metallic openings has inspired great attention since the observation of extraordinary optical transmission (EOT) through a thick metal film perforated with a two-dimensional (2-D) array of subwavelength holes was reported [1]. Due to the vast potential applications of EOT, such as photolithography, optical data storage, organic light-emitting diodes, and photodetectors, many theoretical and experimental studies have been performed in understanding the interaction of light with metals in various subwavelength structures [2]-[4]. In general, the finite-difference time-domain (FDTD) method is used for the analysis of periodic metallic gratings. However, the surface plasmon polaritons (SPPs) are highly localized along the metal-dielectric interface. To simulate the effect of SPPs accurately, fine spatial mesh should be used in this interface region. This result in an extremely small time step by the Courant-Friedrich-Levy (CFL) constraint [5], causing a long computing time. To remove this limitation in simulation, some unconditionally stable FDTD methods were introduced [6]-[9]. Recently, a new unconditionally stable FDTD method based on the Newmark-Beta algorithm has been proposed [10]. For large or multiscale problems with a tremendous number of unknowns, however, the calculation of its large and sparse linear equations leads to a heavy computation burden.

A promising solution for the calculation of large-scale matrices is the domain decomposition (DD) scheme [11-13]. In this paper, an efficient DD scheme is originally introduced into Newmark-Beta-FDTD for the analysis of two-dimensional (2-D) dispersive metallic gratings. As SPPs are highly localized near the metal-dielectric interfaces, graded grids with the fine spatial size are used for accuracy. A number of FDTD-based algorithms for the analysis of dispersive materials have already been proposed in literature, such as the auxiliary differential equation (ADE) method [5], the Z-transform method [14], and the method based on the discrete convolution of the dispersion relation [15]. Since the ADE method offers a more general representation for the dispersion relation, it is employed to simulate the dispersion effect caused by SPPs. The DD-Newmark-Beta-FDTD method decomposes the whole computational domain into several small subdomains. With the theory of Schur complement system, the solution of the large-scale matrix can be converted to the solutions of some small independent ones. With the reverse Cuthill-Mckee (RCM) technique to preprocess the coefficient matrix in each subsystem before performing the lower-upper (LU) decomposition, the small linear systems can be solved efficiently. The EOT through a periodic metallic grating is investigated, and the results verify the efficiency and accuracy of the proposed method.

II. NUMERICAL FORMULATION

The formulation of the Newmark-Beta-FDTD

Submitted On: June 27, 2017
Accepted On: June 13, 2018

method based on the ADE technique has been presented in [16]. The dispersion relation of the Drude medium is given by:

$$\varepsilon(\omega)=1-\frac{\omega_{\mathrm{p}}^{\,2}}{\omega(\omega+\mathrm{i}\gamma)}, \tag{1}$$

where ω_{p} is the plasma frequency, γ is the absorption coefficient, and ω is the angular frequency of the wave.

Here, the implementation process of ADE-Newmark-Beta-FDTD in domain decomposition will be elaborated in detail. Without loss of generality, the whole computational domain is decomposed into four subdomains, marked as D_1, D_2, D_3, and D_4, and the interfaces between neighboring subdomains are named as Γ_{12}, Γ_{14}, Γ_{23}, and Γ_{34}, as shown in Fig. 1. For a specific simulated structure, different size grids can be adopted in different subdomains. For simplicity, the uniform mesh is used for all subdomains in Fig. 1, and the information in adjacent subdomains can be directly coupled by the interfaces.

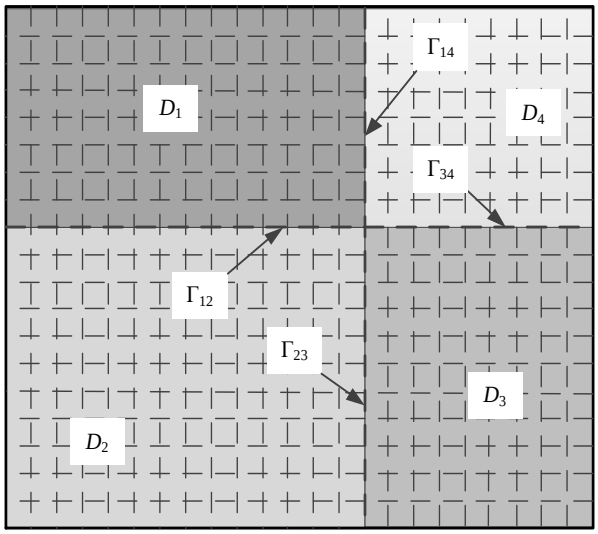

Fig. 1. Four subdomains in a 2-D computational domain.

For the original system, the implicit updated matrix equation in Newmark-Beta-FDTD can be written as:

$$\boldsymbol{A}\boldsymbol{H}_z^{n+1}=\boldsymbol{b}^n, \tag{2}$$

where $\boldsymbol{A}$ is a large banded-sparse matrix. After the whole computational domain is divided into four subdomains, the unknowns, namely the magnetic field variables on the grids, are reordered starting with those in D_1, followed by those in D_2, D_3, and D_4, and ending with those on interfaces. We use n_i (i = 1, 2, 3, and 4) to represent the number of unknowns in each subdomain and n_Γ to represent the number of unknowns on the interfaces, where $\Gamma=\Gamma_{12}\cup\Gamma_{14}\cup\Gamma_{23}\cup\Gamma_{34}$. Thus, the new matrix system is written as:

$$\begin{bmatrix} \boldsymbol{A}_{11} & 0 & 0 & 0 & \boldsymbol{A}_{1\Gamma} \\ 0 & \boldsymbol{A}_{22} & 0 & 0 & \boldsymbol{A}_{2\Gamma} \\ 0 & 0 & \boldsymbol{A}_{33} & 0 & \boldsymbol{A}_{3\Gamma} \\ 0 & 0 & 0 & \boldsymbol{A}_{44} & \boldsymbol{A}_{4\Gamma} \\ \boldsymbol{A}_{\Gamma 1} & \boldsymbol{A}_{\Gamma 2} & \boldsymbol{A}_{\Gamma 3} & \boldsymbol{A}_{\Gamma 4} & \boldsymbol{A}_{\Gamma\Gamma} \end{bmatrix} \begin{bmatrix} \boldsymbol{H}_{z1} \\ \boldsymbol{H}_{z2} \\ \boldsymbol{H}_{z3} \\ \boldsymbol{H}_{z4} \\ \boldsymbol{H}_{z\Gamma} \end{bmatrix} = \begin{bmatrix} \boldsymbol{b}_1 \\ \boldsymbol{b}_2 \\ \boldsymbol{b}_3 \\ \boldsymbol{b}_4 \\ \boldsymbol{b}_\Gamma \end{bmatrix}, \tag{3}$$

where $\boldsymbol{A}_{ii}$ corresponds to the interior-to-interior system, $\boldsymbol{A}_{i\Gamma}$ corresponds to the interior-to-interface coupling between D_i and Γ, $\boldsymbol{A}_{\Gamma i}$ corresponds to the interface-to-interior coupling between Γ and D_i, and $\boldsymbol{A}_{\Gamma\Gamma}$ corresponds to the interface-to-interface contribution. The vectors of $\boldsymbol{H}_{zi}$ and $\boldsymbol{H}_{z\Gamma}$ represent the magnetic field components corresponding to the subdomain D_i and interface Γ, respectively. And the vectors $\boldsymbol{b}_i$ and $\boldsymbol{b}_\Gamma$ are known terms in accordance with $\boldsymbol{H}_{zi}$ and $\boldsymbol{H}_{z\Gamma}$. The orders of $\boldsymbol{A}_{ii}$ and $\boldsymbol{A}_{i\Gamma}$ are $n_i \times n_i$ and $n_i \times n_\Gamma$, respectively. To elaborate the matrix generation in each subdomain, the implicit updated equation of H_z in [16] is rewritten here:

$$\begin{aligned}
&\left[\frac{\mu_0}{2\Delta t}+C\left(\frac{1}{2\Delta y^2}+\frac{1}{2\Delta x^2}\right)\right]H_z\Big|_{i+\frac{1}{2},j+\frac{1}{2}}^{n+1} \\
&-\frac{C}{4\Delta y^2}\left(H_z\Big|_{i+\frac{1}{2},j+\frac{3}{2}}^{n+1}+H_z\Big|_{i+\frac{1}{2},j-\frac{1}{2}}^{n+1}\right) \\
&-\frac{C}{4\Delta x^2}\left(H_z\Big|_{i+\frac{3}{2},j+\frac{1}{2}}^{n+1}+H_z\Big|_{i-\frac{1}{2},j+\frac{1}{2}}^{n+1}\right) \\
&=\frac{\mu_0}{2\Delta t}H_z\Big|_{i+\frac{1}{2},j+\frac{1}{2}}^{n-1} \\
&+\frac{C}{\Delta y}\left(E_x\Big|_{i+\frac{1}{2},j+1}^{n+1}-E_x\Big|_{i+\frac{1}{2},j}^{n+1}\right)-\frac{C}{\Delta x}\left(E_y\Big|_{i+1,j+\frac{1}{2}}^{n+1}-E_y\Big|_{i,j+\frac{1}{2}}^{n+1}\right) \\
&+\frac{1}{2\Delta y}\left(E_x\Big|_{i+\frac{1}{2},j+1}^{n}-E_x\Big|_{i+\frac{1}{2},j}^{n}\right)-\frac{1}{2\Delta x}\left(E_y\Big|_{i+1,j+\frac{1}{2}}^{n}-E_y\Big|_{i,j+\frac{1}{2}}^{n}\right) \\
&+\frac{1}{4\Delta y}\left(E_x\Big|_{i+\frac{1}{2},j+1}^{n-1}-E_x\Big|_{i+\frac{1}{2},j}^{n-1}\right)-\frac{1}{4\Delta x}\left(E_y\Big|_{i+1,j+\frac{1}{2}}^{n-1}-E_y\Big|_{i,j+\frac{1}{2}}^{n-1}\right)
\end{aligned}, \tag{4}$$

where

$$C=\frac{2\Delta t+\gamma\Delta t^2}{4\varepsilon+2\varepsilon\gamma\Delta t+\varepsilon_0\Delta t^2\omega_{\mathrm{p}}^2}, \tag{5}$$

ε and ε_0 are the electric permittivity of the medium and free space, respectively, μ_0 is the magnetic permeability, γ is the absorption coefficient, and ω_p is the plasma frequency.

Since the magnetic field is updated in an implicit way, the interface between difference subdomains is placed on the location of H_z. Taking $\boldsymbol{A}_{22}$ and $\boldsymbol{A}_{2\Gamma}$ in (3) for example, the interface Γ_{23} located at $x = i+5/2$ between D_2 and D_3 is placed on the middle of the grids due to the sample location of magnetic fields, as shown in Fig. 2. As we know, the central difference scheme is adopted in spatial derivatives. For the region $x \le (i+1/2)$, the five magnetic fields in (4) are located in the interior

of D_2 and there is only interior-to-interior coupling between them. So the elements in $\boldsymbol{A}_{22}$ can be filled in the same way as the original implicit matrix. For the magnetic field component H_z (i+3/2, j+1/2), from (4) and Fig. 2, its three neighboring components of H_z (i+3/2, j-1/2), H_z (i+3/2, j+3/2), and H_z (i+1/2, j+1/2) are located in D_2, and their coefficients are loaded in $\boldsymbol{A}_{22}$ normally. However, the component H_z (i+5/2, j+1/2) is located on the interface of Γ_{23}, and its coefficient should be loaded in $\boldsymbol{A}_{2\Gamma}$. The other sub-matrices can be filled in the same way. Moreover, there is no direct coupling between the interior unknowns of any two isolated subdomains due to the center difference scheme in space domain, so the elements in $\boldsymbol{A}_{ij}$ ($i \neq j$) are equal to zero. Besides, it is worth noting that $\boldsymbol{A}_{\Gamma i} = \boldsymbol{A}_{i\Gamma}^{\mathrm{T}}$.

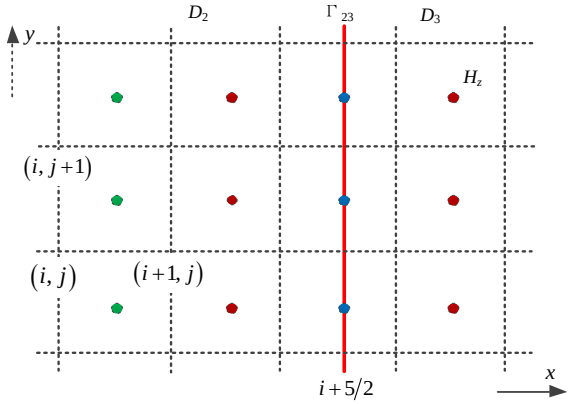

Fig. 2. Local mesh between D_2 and D_3.

While the matrices are filled, we rewrite (3) into several small equations as:

$$\boldsymbol{A}_{11}\boldsymbol{H}_{z1} + \boldsymbol{A}_{1\Gamma}\boldsymbol{H}_{z\Gamma} = \boldsymbol{b}_1, \quad (6a)$$

$$\boldsymbol{A}_{22}\boldsymbol{H}_{z2} + \boldsymbol{A}_{2\Gamma}\boldsymbol{H}_{z\Gamma} = \boldsymbol{b}_2, \quad (6b)$$

$$\boldsymbol{A}_{33}\boldsymbol{H}_{z3} + \boldsymbol{A}_{3\Gamma}\boldsymbol{H}_{z\Gamma} = \boldsymbol{b}_3, \quad (6c)$$

$$\boldsymbol{A}_{44}\boldsymbol{H}_{z4} + \boldsymbol{A}_{4\Gamma}\boldsymbol{H}_{z\Gamma} = \boldsymbol{b}_4, \quad (6d)$$

$$\boldsymbol{A}_{1\Gamma}^T\boldsymbol{H}_{z1} + \boldsymbol{A}_{2\Gamma}^T\boldsymbol{H}_{z2} + \boldsymbol{A}_{3\Gamma}^T\boldsymbol{H}_{z3} + \boldsymbol{A}_{4\Gamma}^T\boldsymbol{H}_{z4} + \boldsymbol{A}_{\Gamma\Gamma}\boldsymbol{H}_{z\Gamma} = \boldsymbol{b}_\Gamma. \quad (6e)$$

From (6a)-(6e), we obtain the updated equation of $\boldsymbol{H}_{z\Gamma}$ as:

$$\left(\boldsymbol{A}_{\Gamma\Gamma} - \sum_{i=1}^{4}\boldsymbol{A}_{i\Gamma}^T\boldsymbol{A}_{ii}^{-1}\boldsymbol{A}_{i\Gamma}\right)\boldsymbol{H}_{z\Gamma} = \boldsymbol{b}_\Gamma - \sum_{i=1}^{4}\boldsymbol{A}_{i\Gamma}^T\boldsymbol{A}_{ii}^{-1}\boldsymbol{b}_i. \quad (7)$$

It is called as the Schur complement system [17] and the coefficient matrix on the left side and the vector on the right side are known. Once the magnetic fields on the interface have been solved from (7), the other magnetic fields in the subdomains can be solved from (6a)-(6d).

It should be noted that (6a)-(6d) are independent from each other, and then, they can be solved in a parallel manner. In order to solve those equations efficiently, the RCM technique is used to reduce the bandwidth of the coefficient matrix, resulting in an efficient LU decomposition. More importantly, the LU decomposition needs to be performed only once at the beginning of the calculation since the coefficient matrix keeps unchanged in the whole time-marching process.

When several small matrix equations are solved independently, much less time and memory are required than solving a large one. Furthermore, if the electromagnetic fields on an interface or in a subdomain are to be obtained, there is no need to solve all the subdomain systems.

III. NUMERICAL RESULTS AND DISCUSSION

To validate the accuracy and efficiency of the proposed DD-Newmark-Beta-FDTD method for solving the multiscale problem with dispersive materials, the transmission resonances of periodic metallic grating structures are investigated in the visible and near infrared regions in this section.

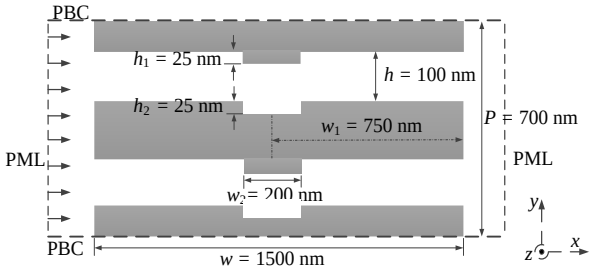

Fig. 3. Schematic of a unit cell of the periodic metallic grating with bumps and cuts.

The unit cell of the periodic metallic grating with bumps and cuts is investigated, as shown in Fig. 3. The computational domain is truncated by the perfectly matched layer (PML) on the left and right sides and periodic boundary condition (PBC) on the top and bottom. A modulated Gaussian pulse is used as the source excitation, and its time variation is given by:

$$F(t) = \sin\left(2\pi f_0 t\right)\cdot \mathrm{e}^{-(t-t_0)^2/\tau^2}, \quad (8)$$

where the center frequency f_0 = 215 THz, $\tau = 1/(2f_0)$ and $t_0 = 3\tau$. The metal loaded on the grating is gold and the considered wavelength range is from 700 nm to 2500 nm. Hence, the corresponding parameters are $\omega_p = 1.37\times10^{16}$ rad/s and $\gamma = 4.08\times10^{13}$ rad/s [18]. To simulate the effect of SPPs around the bumps and cuts accurately, graded cells are used in both x- and y-directions. The minimum cell size is 1 × 0.1 nm^2 and the total cell number of the computational domain is 129 × 176. The traditional FDTD method, the Newmark-Beta-FDTD method, and the proposed DD-Newmark-Beta-FDTD method are employed for this simulation, where $\Delta t_{\mathrm{FDTD}} = 1.6667\times10^{-4}$ fs is chosen for FDTD according to the CFL constraint, while $\Delta t_{\mathrm{Newmark}} = 1100\Delta t_{\mathrm{FDTD}} = 1.8333\times10^{-1}$fs (CFLN = $\Delta t_{\mathrm{Newmark}}/\Delta t_{\mathrm{FDTD}}$ = 1100) is chosen for Newmark-Beta-

FDTD and DD-Newmark-Beta-FDTD. Figure 4 shows that the results of the transmission and reflection spectrums of this grating structure from the three methods, in which the whole computational domain is decomposed into four subdomains for DD-Newmark-Beta-FDTD. From this figure, it can be seen that the results from DD-Newmark-Beta-FDTD are in good agreement with those from FDTD and Newmark-Beta-FDTD. In addition, the transmission spectrum shows the transmission peaks of four waveguide resonances which are associated with different standing wave modes of the slit acting as the Fabry-Pérot (F-P) cavity [19]. Furthermore, compared with the grating without bumps and cuts [16], the transmission peaks for the four resonance modes in the F-P cavity exhibit a red shift. This transmission behavior can be explained by the localized waveguide resonance mode [19]. The resonant wavelength of the F-P mode in a smooth slit array is given by $2kL_{FP}+\theta = 2N\pi$, where $k = 2n\pi/\lambda$ is the wave number (λ is the wavelength of the Nth order mode, and n is the effective refractive index of the fundamental Bloch mode propagating in the slit), L_{FP} is the length of the cavity, and θ, an N-dependent value, is the total phase reflected at the ends of the slits. The loading of the perpendicular bumps and cuts enlarges the effective length of F-P cavity for both odd and even modes. Hence, the resonance wavelengths of all modes become large and show a red shift. This method can be used to minimize the volume of the light-wave devices.

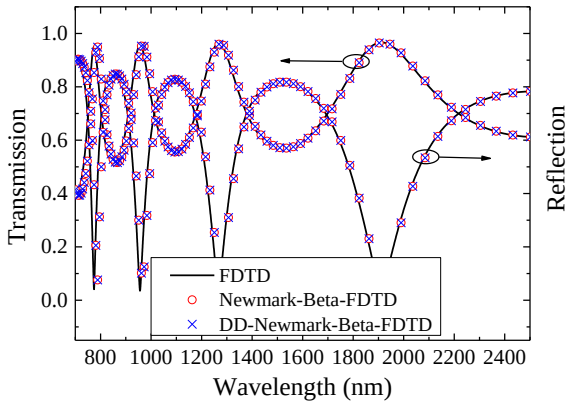

Fig. 4. Transmission and reflection spectrums of the grating with bumps and cuts from FDTD, Newmark-Beta-FDTD (CFLN = 1100), and DD-Newmark-Beta-FDTD (CFLN = 1100 and four subdomains).

In order to evaluate the computational accuracy of those methods, the mean absolute percentage error (MAPE) of the four resonance wavelengths is written as:

$$\text{MAPE}=\frac{1}{4}\sum_{n=1}^{4}\left|\frac{\lambda_{\text{peak}}-\lambda_{\text{peak-FDTD}}}{\lambda_{\text{peak-FDTD}}}\right|\times 100\%, \qquad (9)$$

where $\lambda_{\text{peak-FDTD}}$ is the transmission peaks from FDTD and it acts as the referenced result. Table 1 presents the computational efforts for the three methods, where CFLN = 1100 (MAPE < 1%) of Newmark-Beta-FDTD and DD-Newmark-Beta-FDTD is chosen to guarantee simulation precision. Since the time step of Newmark-Beta-FDTD is chosen 1100 times of FDTD, its CPU time can be reduced to about 1.18% of FDTD, but its memory requirement is about 4.68 times of FDTD. Applying the DD scheme to Newmark-Beta-FDTD with four subdomains, almost 40% of the CPU time and 65% of the memory requirement is saved.

Table 1: Comparison of the computational efforts for the three methods

Method	CFLN	MAPE	CPU Time (s)	Memory (Mb)
FDTD	1	-	51913	33.14
Newmark-Beta-FDTD	1100	0.90%	611	155.24
DD-Newmark-Beta-FDTD (4 subdomains)	1100	0.90%	381	54.64

Table 2: Comparison of the computational efforts for DD-Newmark-Beta-FDTD and Newmark-Beta-FDTD

Method	Domain Number	MAPE	CPU Time (s)	Memory (Mb)
Newmark-Beta-FDTD	1	0.90%	611.46	155.24
DD-Newmark-Beta-FDTD	2	0.90%	467.65	74.59
	3	0.90%	420.62	62.03
	4	0.90%	381.27	54.64
	5	0.90%	347.79	50.43
	6	0.90%	314.80	47.95

Furthermore, the whole computational domain is sequentially decomposed into two to six subdomains along the x-direction for DD-Newmark-Beta-FDTD simulations. With CFLN = 1100, the computational efforts of DD-Newmark-Beta-FDTD and Newmark-Beta-FDTD are compared in Table 2. From this Table, both the CPU time and memory requirement are reduced by using the domain decomposition scheme, and a larger subdomain number results in higher efficiency both in CPU time and memory requirement. The reason is that the LU decomposition of several small matrices costs much less time and memory than a huge one. In addition, it can also be seen from Table 2 that MAPE of DD-Newmark-Beta-FDTDs remains unchanged when the whole computational domain is divided into different subdomains. This is because the DD scheme based on the Schur complement system does not involve any approximation in the calculation process.

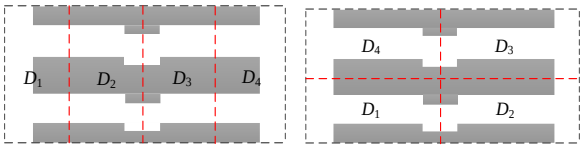

Fig. 5. Two different decomposition structures for four subdomains: (a) Case 1 and (b) Case 2.

Finally, the different spatial structures of the DD scheme are investigated. In the first case, the computational domain of the grating is decomposed into four subdomains with the same number of unknowns along the *x*-direction, as shown in Fig. 5 (a). In the second case, the whole domain is decomposed into four subdomains along the *x*- and *y*-directions, as shown in Fig. 5 (b). Table 3 shows that the computational accuracy and memory requirement of the two cases are the same. However, since the bandwidth of the matrix $\boldsymbol{A}_{i\Gamma}$ in Case 1 is smaller than that in Case 2, Case 1 costs less time in preconditioning coefficient matrices and solving equations.

Table 3: Comparison of the computational efforts for different decomposition structures

Case	Domain Number	MAPE	CPU Time (s)	Memory (Mb)
Case 1	4	0.90%	381.27	54.64
Case 2	4	0.90%	416.59	54.64

IV. CONCLUSION

This work introduces an efficient domain decomposition scheme to the unconditionally stable Newmark-Beta-FDTD method for periodic metallic grating analysis. Since the original computational domain can be decomposed into several small subdomains, the huge matrix equation can be transformed into several small independent ones. With the preconditioning RCM technique to the LU decomposition, which is executed only once at the beginning of the calculation, those small updated equations can be solved independently. The accuracy and efficiency of the proposed method are verified from the numerical example of the periodic metallic grating. The effects of different decomposition structures are also investigated. It has been proved that the DD-Newmark-Beta-FDTD method has high efficiency and low memory requirement while remaining high accuracy. This method is very suitable for the simulation in electrically large size structures involving multiscale grid division, such as photonic gratings, photonic crystals, microwave devices and antennas.

ACKNOWLEDGMENT

This work was supported by the National Natural Science Foundation of China (No. 61471105 and 6133107).

REFERENCES

[1] T. W. Ebbesen, H. J. Lezec, H. F. Ghaemi, T. Thio, and P. A. Wolff, "Extraodinary optical transmission through sub-wavelength hole arrays," *Nature*, vol. 391, no. 6668, pp. 667-669, Feb. 1998.

[2] C. Genet and T. W. Ebbesen, "Light in tiny holes," *Nature*, vol. 445, no. 7123, pp. 39-46, Jan. 2007.

[3] J. A. Porto, F. J. Garcia-Vidal, and J. B. Pendry, "Transmission resonance on metallic gratings with very narrow slits," *Phy. Rev. Lett.*, vol. 83, no. 14, pp. 2845-2848, Oct. 1999.

[4] H. J. Lezec and T. Thio, "Diffracted evanescent wave model for enhanced and suppressed optical transmission through subwavelength hole arrays," *Opt. Exp.*, vol. 12, no. 16, pp. 3629-3651, Aug. 2004.

[5] A. Taflove and S.C. Hagness, *Computational Electrodynamics: The Finite-Difference Time-Domain Method*. Norwood, MA: Artech House, 2000.

[6] T. Namiki, "A new FDTD algorithm based on alternating-direction implicit method," *IEEE Trans. Microw. Theory Techn.*, vol. 47, no. 10, pp. 2003-2007, Oct. 1999.

[7] L. Gao, B. Zhang, and D. Liang, "The splitting finite difference time-domain methods for Maxwell's equations in two dimensions," *J. Comput. Appl. Math.*, vol. 205, no. 1, pp. 207-230, Aug. 2007.

[8] E. L. Tan, "Unconditionally stable LOD-FDTD method for 3-D Maxwell's equations," *IEEE Microw. Wireless Compon. Lett.*, vol. 17, no. 2, pp. 85-87, Feb. 2007.

[9] G. Sun and C. W. Truneman, "Efficient implementations of the Crank-Nicolson scheme for the finite-difference time-domain method," *IEEE Trans. Microw. Theory Techn.*, vol. 54, no. 5, pp. 2275-2284, May 2006.

[10] S. B. Shi, W. Shao, X. K. Wei, X. S. Yang, and B. Z. Wang, "A new unconditionally stable FDTD method based on the Newmark-Beta algorithm," *IEEE Microw. Theory Techn.*, vol. 64, no. 12, pp. 4082-4090, Dec. 2016.

[11] M. N. Vouvakis, Z. Cendes, and J. F. Lee, "A FEM domain decomposition method for photonic and electromagnetic band gap structures," *IEEE Trans. Antennas Propag.*, vol. 54, no. 2, pp. 721-733, Feb. 2006.

[12] B. Z. Wang, R. Mittra, and W. Shao, "A domain decomposition finite-difference utilizing characteristic basis functions for solving electrostatic problems," *IEEE Trans. Electromagn. Compat.*, vol. 50, no. 4, pp. 946-952, Nov. 2008.

[13] G. Q. He, W. Shao, X. H. Wang, and B. Z. Wang, "An efficient domain decomposition Laguerre-FDTD method for two-dimensional scattering

problems," *IEEE Trans. Antennas Propag.*, vol. 64, no. 5, pp. 2639-2645, May 2013.
[14] D. Sullivan, "Nonlinear FDTD formulations using Z transforms," *IEEE Trans. Microw. Theory Techn.*, vol. 43, no. 3, pp. 676-682, Mar. 1995.
[15] R. J. Luebbers and F. Hunsberger, "FDTD for *N*th-order dispersive media," *IEEE Trans. Antennas Propag.*, vol. 40, no. 11, pp. 1297-1301, Nov. 1992.
[16] S. B. Shi, W. Shao, T. L. Liang, L. Y. Xiao, X. S. Yang, and H. Ou, "Efficient frequency-dependent Newmark-Beta-FDTD method for periodic grating calculation," *IEEE Photonics J.*, vol. 8, no. 6, pp. 1-9, Dec. 2016.
[17] T. N. Phillips, "Preconditioned iterative methods for elliptic problems on decomposed domains," *Int. J. Comput. Math.*, vol. 44, pp. 5-18, 1992.
[18] E. D. Palik, *Handbook of Optical Constants in Solids*. Academic, 1982.
[19] A. P. Hibbins, M. J. Lockyear, and J. R. Sambles, "The resonant electromagnetic fields of an array of metallic slits acting as Fabry-Pérot cavities," *J. Appl. Phys.*, vol. 99, no. 12, pp. 1-5, June 2006.

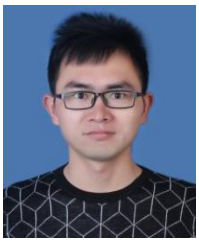

Sheng-Bing Shi was born in Hubei, China, in 1990. He received the B.S. degree in Physics from the Yangtze University, Jingzhou, China, in 2013. In 2015, he received the M.S. degree in Radio Physics at University of Electronic Science and Technology of China (UESTC). Currently, he is working toward the Ph.D. degree in Radio Physics at UESTC.

His research interest is computational electromagnetics.

Wei Shao received the B.E. degree in Electrical Engineering, and the M.Sc. and Ph.D. degrees in Radio Physics from the University of Electronic Science and Technology of China (UESTC), Chengdu, in 1998, 2004, and 2006, respectively. He joined the UESTC in 2007. From 2010 to 2011, he was a Visiting Scholar with the Electromagnetic Communication Laboratory, Pennsylvania State University, State College, PA, USA. He is currently a Professor with UESTC.

His current research interests include computational electromagnetics and antenna design.

Kai Wang was born in Sichuan, China, in 1992. He received his B.E. degree in Electronic Information Science and Technology from the University of Electronic Science and Technology of China (UESTC) in 2015. He is working toward the M.S. degree in Radio Physics at UESTC. His research interest is computational electromagnetics.